AIAA JOURNAL
Vol. 43, No. 9, September 2005

Drag Reduction of a Near-Sonic Airplane by Using Computational Fluid Dynamics

Wataru Yamazaki,* Kisa Matsushima,† and Kazuhiro Nakahashi‡
Tohoku University, Sendai 980-8579, Japan

Aerodynamic shape optimization for an airplane cruising at a near-sonic regime is discussed based on computational fluid dynamics. Japan Aerospace Exploration Agency's scaled experimental supersonic airplane model, NEXST-1, was employed as the baseline model of the optimization. NEXST-1 was accepted as a candidate for a near-sonic airplane because of the existence of a "drag bucket" at a near-sonic regime, as shown by the past research of the present authors. In the present optimization, the section airfoil shape and the planform shape were optimized independently of each other in the near-sonic regime of Mach number 0.98. For the optimization, a genetic algorithm was used with unstructured mesh Euler simulations. The results of the optimizations showed considerable improvement in the lift-to-drag ratio in the near-sonic regime. The optimization of the section airfoil shape and that of the planform shape yielded to the reduction of wave drag and induced drag, respectively.

Nomenclature

a	=	local sonic speed
C_{Df}	=	friction drag coefficient
C_{DP}	=	pressure drag coefficient
C_L	=	lift coefficient
Cp	=	pressure coefficient
D or O	=	switching factor of planform shape's type
e	=	Oswald efficiency factor
$\boldsymbol{F}_{\mathrm{shock}}$	=	shock function
P	=	pressure
S_{ref}	=	reference area
TW	=	twist angle modification variables
t/c	=	nondimensional thickness of airfoil
$\boldsymbol{V}$	=	velocity vector

I. Introduction

RECENTLY, with the globalization of trading, human activity, and transportation, the reduction of flight time between continents is demanded. In Japan, for the realization of next-generation high-speed airplanes, a national experimental supersonic transport (NEXST),[1–3] which was a 1/10-scaled experimental airplane, was developed at the Japan Aerospace Exploration Agency (JAXA). With present technology, however, it is pointed out that supersonic transport (SST) faces some difficulties such as fuel inefficiency, noise pollution, air pollution, and sonic boom. Because of the present situation, an airplane cruising at a near-sonic regime is watched with keen interest. Because its cruising speed is about 15% greater than that of present transonic airplanes, this results in a considerable increase in transportation efficiency. Moreover, the absence of sonic boom with near-sonic cruising is an attractive advantage from an environmental standpoint.

In research related to near-sonic airplanes, wind-tunnel tests of several airfoils in the near-sonic regime were conducted in the 1950s by the NACA in the United States.[4] In the 1970s, along with the research on supercritical airfoils, near-sonic airplanes attracted attention, and development of a near-sonic airplane was attempted at the Aircraft Research Association in the United Kingdom.[5] In that research, development of a near-sonic airplane was attempted based on the geometry of a conventional transonic airplane. Unfortunately, it was not realized at that time because of increases in the cost of fuel.

As the most well-known case of a recent near-sonic airplane, Sonic-Cruiser,[§] which the Boeing Company had investigated and challenged the development of, is well known. The configuration of Sonic-Cruiser had several new features such as canards, rear-mounted engines, and two horizontal fins at the back of the airplane. The novel shape attracted the attention of researchers as well as the public. Later, however, this configuration was seemed to be modified by Boeing researchers to a nearly conventional one according to the 24–30 September 2002 issue of *Flight International*.[6] Unfortunately, because of the negative influence on aviation by terrorism, recent economic sluggishness and so on, the development of a sonic-cruiser was suspended in 2002. However, the near-sonic airplane is thought to be well worth analyzing for the future possibility of its realization as a commercial airplane, as well as for opportunities such analysis might offer the discovery of some useful knowledge about near-sonic flow.

Regarding the aerodynamics of the near-sonic airplane, it is difficult to prevent the generation of shock waves in the near-sonic regime. Therefore, the reduction of wave drag or control of shock waves will be a key for the realization of a near-sonic airplane from the aerodynamic point of view. So as our design perspective on a near-sonic airplane, it was suggested by the present authors that a supersonic airplane might be a good candidate for the baseline model of a near-sonic airplane. Thus, inspection of the aerodynamics and the preliminary design at the near-sonic regime was conducted using an SST model.[7,8] In these research studies, JAXA's experimental SST model, called NEXST-1 (Fig. 1), was used. A minimum drag region, called "drag bucket," was observed in the near-sonic regime by these research studies. This phenomenon enhanced the possibility of using the NEXST-1 model as the baseline model of a near-sonic airplane.

Considering the just-mentioned phenomenon together with the past work in the 1970s, what is the most suitable shape and important factor for an efficient near-sonic cruising? In this paper, aerodynamic shape optimization at the near-sonic regime based on the NEXST-1 SST model is examined using computational-fluid-dynamics (CFD) simulations. The optimization of the section airfoil shape and that

Presented as Paper 2004-0034 at the AIAA 42nd Aerospace Sciences Meeting, Reno, NV, 5–8 January 2004; received 27 December 2004; revision received 1 April 2005; accepted for publication 3 April 2005.

*Graduate Student, Department of Aerospace Engineering. Student Member AIAA.

†Associate Professor, Department of Aerospace Engineering. Senior Member AIAA.

‡Professor, Department of Aerospace Engineering. Associate Fellow AIAA.

§Data available online at http://www.boeing.com [cited 24 December 2004].

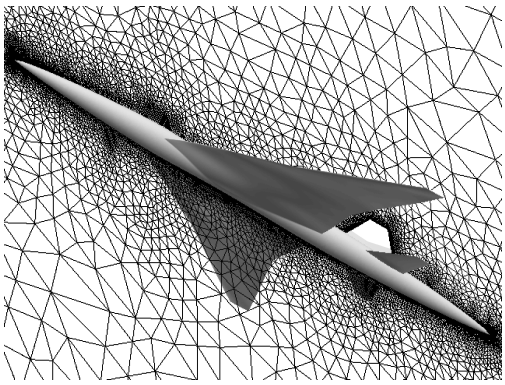

Fig. 1 NEXST-1 SST model with unstructured mesh.

of the planform shape were conducted separately. From the results of these optimizations, the reasons for drag reduction and the aerodynamics, especially the phenomena around the shock waves, were analyzed in detail.

II. Computational Methods

In this section, computational methods used in this research are concisely introduced.

A. Optimization Method

In aerodynamic optimization, for the treatment of complicated flows, the nonlinearity of the objective functions must be taken into consideration. So a genetic algorithm (GA) was adopted in this research because it did not require the derivatives of the objective functions. GA simulates the evolutional process of creatures. It is a population-based optimization method, in which the population evolves over generations to minimize/maximize objective functions by the operations of selection, crossover, and mutation.[9] In this research, GA of optimization commercial software modeFRONTIER[¶] was applied.

B. Aerodynamic Evaluation

In this research, a flow solver named TAS-Code (Tohoku University Aerodynamic Simulation), which is based on the three-dimensional unstructured mesh method, was used to evaluate aerodynamic performance. In the simulation code, Euler/Navier–Stokes (NS) equations were solved by a finite volume cell-vertex scheme. The numerical flux normal to the control volume boundary was computed using an approximate Riemann solver of Harten–Lax–van Leer–Einfelds–Wada.[10] Second-order spatial accuracy was realized by a linear reconstruction of the primitive gas dynamic variables inside the control volume with Venkatakrishnan's limiter.[11] The lower/upper symmetric Gauss–Seidel (LU-SGS) implicit method for unstructured meshes[12] was used for the time integration.

The mesh of the NEXST-1 model for the Euler computation was all tetrahedrons, and a mesh that had about 300,000 nodes, shown in Fig. 1, was generally used in this research. The surface mesh was generated by the advancing front method of a graphical-user-interface-based user interactive tool, called TAS-Mesh.[13] The volume mesh was generated by the Delaunay approach.[14] For the NS computation, a hybrid volume mesh[15] composed of tetrahedrons, prisms, and pyramids was used, and a mesh that had about 1.4 millions nodes was generally used in this research. A one-equation turbulence model by Goldberg and Ramakrishnan[16] was adopted to treat turbulent boundary layers.

By the use of such unstructured meshes, NS computation required CPU time about 20 times more than that by Euler computation. In our past research,[7] it was confirmed that the tendency of the aerodynamic coefficients variation was basically the same between the computational results of Euler and NS in the near-sonic regime. Moreover, these results also showed good agreement with experimental data.[8] This implied that the interference between the shock waves and the boundary layer was weak in this regime. It is the best to adopt NS computation for aerodynamic evaluation in the optimization process from the viewpoint of the accuracy, but GA will require a huge number of aerodynamic evaluations in the process. Therefore, Euler computation was adopted as the evaluation method of the aerodynamic performance considering the balance between computational cost efficiency and required accuracy for the present optimization.

[¶]Data available online at http://www.esteco.it [cited 24 December 2004].

C. Reduction of Computational Time for Mesh Generation

As just mentioned, GA will require a huge number of aerodynamic evaluations of different shape airplanes, as well as a huge number of regenerations of unstructured mesh. Therefore, in the first optimization case, which is a section airfoil shape optimization discussed in the next chapter, this mesh-regeneration process was avoided by applying a mesh-movement method based on a spring analogy[17] to NEXST-1's unstructured mesh. In the second case, a planform shape optimization discussed in a later section, the extent of required geometry modification was beyond the capability of the mesh-movement method. In this optimization for the latter case, therefore, an automatic surface and volume mesh-regeneration system based on the Delaunay triangulation approach was constructed and applied. By the use of these methods, the regeneration process of unstructured mesh was improved and could be conducted automatically with an acceptable computational cost.

III. Section Airfoil Shape Optimization

A. Optimization Problem Definitions

1. Geometry Definitions

In this chapter, the section airfoil shape of the NEXST-1 model, including the camber, thickness, and twist angle distributions, was optimized. The wing root, which was 15% of the semispan of the wing and the wing planform shape, was fixed. The total number of design variables was 66. In detail, the design variables were distributed at six semispan stations, 25%, 40% (kink of trailing edge), 50% (kink of leading edge), 70%, 85%, and 100%. For each airfoil shape, the upper and lower surface geometries were respectively modified by the use of five control points on each surface and spline curve fitting. In addition, the airfoil shape and the twist angle distribution along the spanwise direction were interpolated by spline curve fitting using the six semispan stations as the spanwise control points. The outline of the geometry definition is shown in Fig. 2.

2. Objective and Constraints for the Optimization

The objective was to minimize C_{DP} at Mach number 0.98. C_{DP} was evaluated by Euler computation. To prevent a design having a lower drag yielded to by lowering lift, the constraint that C_L kept constant (0.26) was set. This was attained by adjusting the angle of attack based on the comparison of the current C_L and the target C_L every 100 time steps of LU-SGS iteration during the numerical simulation. The simulation program can perform the C_L adjustment

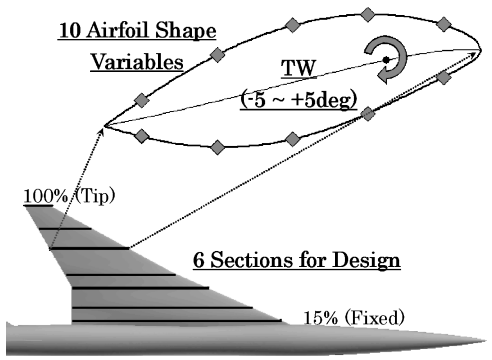

Fig. 2 Design variables definition for section airfoil shape optimization.

automatically. Moreover, to prevent drag reduction by a mere thinner wing generation, a constraint that wing volume should be greater than that of NEXST-1 was also set. A design that did not satisfy these constraints could not survive to the next generation in the optimization process of GA.

B. Results and Discussion

The population size at each generation of GA was set to be 30, and the probability of mutation was 0.1. All initial individuals were randomly generated. The computation was done until the 70th generation, and so about 2100 flow simulations of different shaped airplanes were required. The computation time was about 1 h per 1 design by NEC SX-7 of the Supercomputing System Information Synergy Center at Tohoku University. The history of the optimization, including the maximum, average, and minimum value of the objective function in each generation, is shown in Fig. 3. It can be seen that the optimization almost reached a convergence state. Comparison of the aerodynamic performance of NEXST-1 and the obtained optimal design is shown in Table 1 (with the evaluation category "Euler"). A 37-count reduction (1 count = 0.0001) of C_{DP} was achieved by the optimization. A detailed comparison between the NEXST-1 model and the obtained optimal design will be presented in the following section.

1. Comparison About the Geometry

The geometrical contour of the upper surface of the wing is shown in Fig. 4. Each contour line indicates the height of the wing upper surface. It was confirmed that small dips appeared on the upper surface of the outboard wing at the optimal design. It was also observed in the optimal design that the section airfoil camber increased at most span stations and that the twist angle decreased overall compared with that of NEXST-1. Section area distributions of the wing with the fuselage normal to the freestream flow direction are shown in Fig. 5 for the investigation of the contribution of the area rule. It was confirmed that the distribution of the NEXST-1 model as well as that of the obtained optimal design was satisfactorily smooth. Therefore, it was considered that the NEXST-1 model was already optimized from the viewpoint of the area rule, and the small dips of the optimal design were not created for the improvement of the smoothness of the section area distribution.

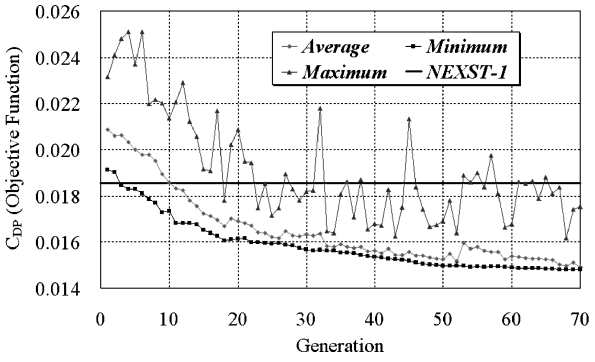

Fig. 3 History of section airfoil shape optimization.

2. Comparison About the Aerodynamics

Shock visualization based on the following shock function is shown in Fig. 6. $\boldsymbol{F}_{\text{shock}}$ is given as follows:

$$\boldsymbol{F}_{\text{shock}} = (\boldsymbol{V} \cdot \nabla \boldsymbol{P})/(\boldsymbol{a} \cdot |\nabla \boldsymbol{P}|) \tag{1}$$

It is known that the positive region of this function corresponds to the compression region, and that where the function is negative, it is an expansion region. Moreover, the zone in which $\boldsymbol{F}_{\text{shock}} \geq 1$ in the compression region is the upstream zone of a shock wave.[18] In the Fig. 6, only this upstream zone of shock waves is visualized with entropy production. It can be seen that the shock waves on the outboard wing vanished in the present optimal design. It was considered that this disappearance of the shock waves was related to the dips of the wing upper surface, shown in Fig. 4. That is, by letting an airfoil surface be wavy, compression and expansion waves

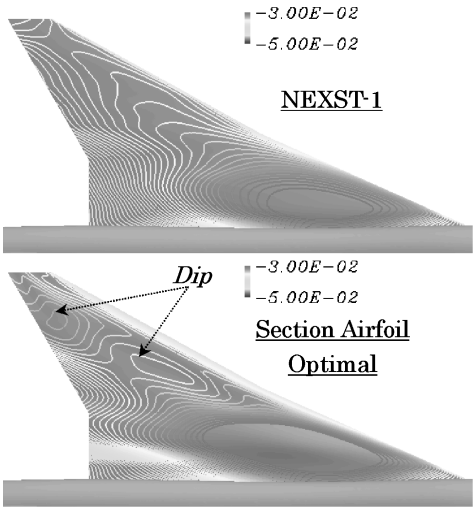

Fig. 4 Geometrical contour of wing upper surface.

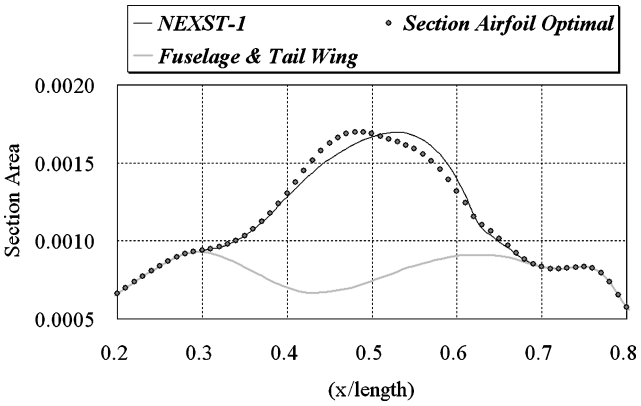

Fig. 5 Area rule investigation for the section airfoil shape optimization.

Table 1 Comparison of the aerodynamic performance of section airfoil shape optimization

Design	Wing volume	Evaluation	AoA, deg[a]	C_L	C_{DP}	C_{Df}	L/D
NEXST-1	1.000	Euler	3.48	0.26	0.01855	——	14.02
		Euler-fine	3.31	0.26	0.01749	——	14.86
		NS	3.46	0.26	0.01965	0.01078	8.56
Section airfoil optimal	1.003	Euler	4.02	0.26	0.01481	——	17.56
					−37 counts		+25%
		Euler-fine	3.87	0.26	0.01380	——	18.84
					−37 counts		+27%
		NS	4.24	0.26	0.01596	0.01093	9.68
					−37 counts		+13%

[a]AoA = angle of attack.

were effectively generated. These waves then interfered with each other to form a well-combined wave pattern, which contributed to the disappearance of shock waves on the outboard wing. Moreover, it was confirmed that the entropy production at the inner wing caused by shock waves was also reduced in the optimal design.

For the investigation of the reduction of the shock strength, shock function visualizations at the 40% semispan station are shown in Fig. 7. Only compression regions are indicated. Although the upstream region of shock wave was almost expansion region in the NEXST-1 model, it was found that compression regions appeared upstream of the primary shock wave in the obtained optimal design. This result showed that shockless smooth, that is, isentropic compression at upstream of the shock wave, contributed to the reduction of shock strength in the optimal design. Comparison of the Cp distributions at the 40% semispan station of the NEXST-1 and the optimal design is shown in Fig. 8. Reduction of the shock strength was found to be remarkable, and the Cp distribution was modified to the rear-loading type in the optimal design.

The lift and pressure drag force distributions in the spanwise direction are plotted in Fig. 9. The spanwise lift distribution was basically the same in both the NEXST-1 and the optimal design. In the pressure drag plot, on the other hand, the drag reduction of the optimal design in the outboard wing was remarkable. Especially, the pressure drag force in this region was below zero, and so it acted as a thrust force. For analysis of this thrust phenomenon, comparison of the Cp-x and Cp-z distributions at the 85% semispan station, exactly the just-mentioned thrust position, is shown in Fig. 10, where x and z mean the parallel and vertical coordinate in the freestream flow direction, respectively. Thus, the area surrounding the loop of the Cp-x and Cp-z indicates the lift and pressure drag force, respectively. The position of the pressure recovery on the upper surface is indicated in this figure. It was confirmed from the Cp-z plot that a large thrust loop was generated by the effect of pressure recovery on the upper surface, which occurred near the position of the upper crest of the wing in the optimal design. That is to say, by the optimized position of the pressure recovery, the low pressure before the upper crest of the wing and the recovered pressure behind the crest both contributed to the thrust force production.

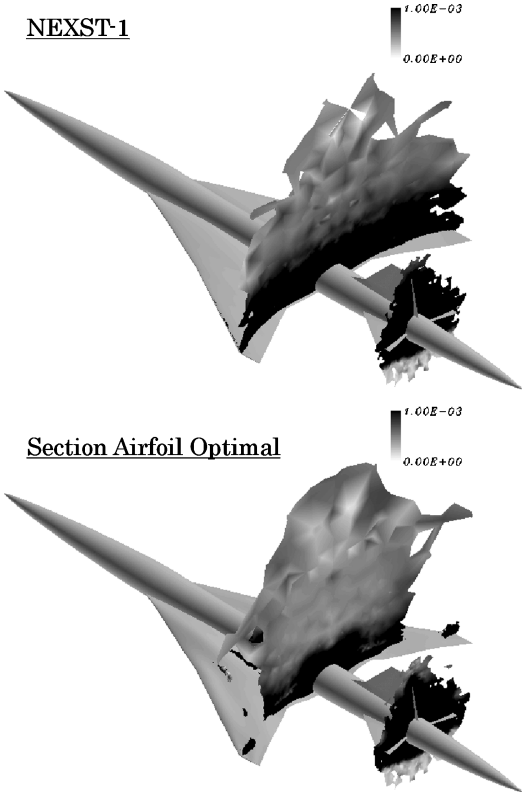

Fig. 6 Shock and entropy visualization.

IV. Planform Shape Optimization

A. Optimization Problem Definitions

Section airfoil shape optimization conducted in the preceding section showed good improvement in the lift-to-drag ratio (L/D). The optimized value of the L/D, however, was still insufficient for efficient cruising in the near-sonic regime, and further optimization in a larger design space was required. In this section, therefore, aerodynamic optimization of the planform shape is discussed.

1. Geometry Definitions

Optimization of the wing planform shape is discussed in this chapter. For the fuselage and the tail wing of a new airplane, the shapes of those of the NEXST-1 SST model were retained. The wing-fuselage junction geometry was also fixed for the sake of simplicity of the generation of the computational mesh and for reduction of the number of design variables. The outline of the parametric definition

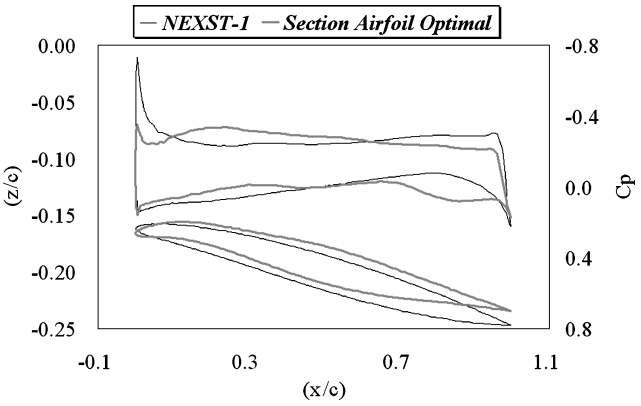

Fig. 8 *Cp* distribution of section airfoil optimal design at 40% semispan.

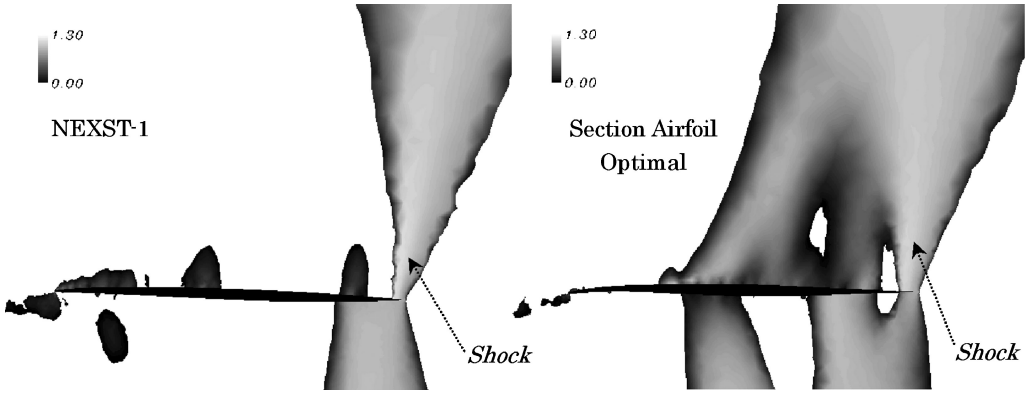

Fig. 7 Shock function visualization at 40% semispan.

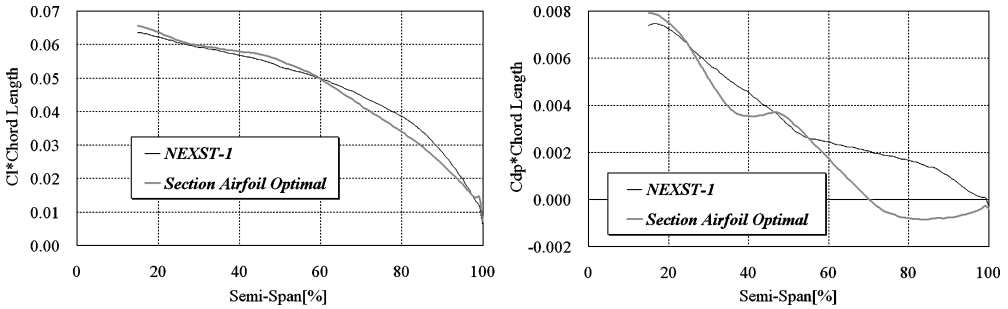

Fig. 9 Lift and pressure drag distributions of section airfoil optimal design in the spanwise direction.

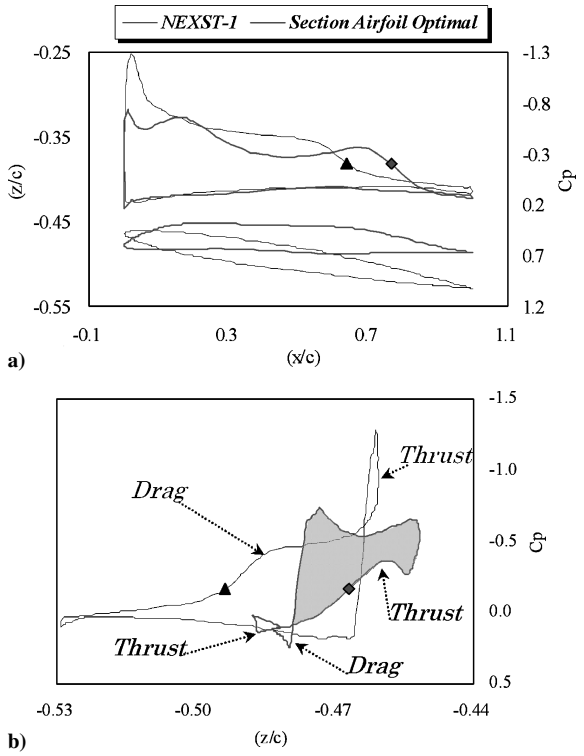

Fig. 10 *Cp* distribution of section airfoil optimal design at 85% semispan: a) *Cp-x* plot and b) *Cp-z* plot.

of the planform shape based on the design variables is shown in Fig. 11. The basic shape of the planform was defined by five design variables: the length of the x direction from the wing root to the wing kink X_{kink}, the semispan length of the inboard wing Y_{kink}, the chord length at the kink C_{kink}, the length of the x direction from the wing root to the wing tip X_{tip}, and the semispan length of the outboard wing Y_{tip}. Then the front line of the planform shape, which corresponded to the leading-edge line, was determined by the three control points (fixed root, free kink, and tip position of the leading edge) using linear or spline curve interpolation. The linear interpolation resulted in a double-delta wing planform, whereas the spline interpolation resulted in an Ogee wing. The selection of the interpolation method was decided by another design variable D or O. The chord length at the wing tip was calculated automatically according to the given condition of the S_{ref} constant.

The section airfoil shape was determined by the following rule: the shape of the airfoil should be similar to that of the NEXST-1 model at the corresponding semispan station. This rule was adopted to reduce the number of design variables relating to the section airfoil shape. This treatment of the section airfoil shape also made the t/c at every span station constant during the optimization. Thus, it was unnecessary to consider the possibility of designing a thinner airfoil shape. Initially, the twist angle distribution of a new modified airplane was set to be same as that of NEXST-1. Then the twist angle

Table 2 Acceptable range of design variables

Parameter	Range
Fuselage length	$L = 1.0$ (unit length)
Chord length @root	$C_{\text{root}} \sim 0.333$ (fixed)
Reference wing area	$S_{\text{ref}} = 0.03826$ (fixed)
Inboard span length	$0.02 < Y_{\text{kink}} < 0.15$
Outboard span length	$0.02 < Y_{\text{tip}} < 0.15$
Chord length @kink	$0.05 < C_{\text{kink}} < 0.25$
X coordinate @kink	$0 < X_{\text{kink}} < 0.457$
X coordinate @tip	$0 < X_{\text{tip}} < 0.457$
Modification range of twist angle	-5 deg $<$ TW $<$ $+5$ deg

distribution was modified using the spline curve technique by four design variables TW, which were distributed at the 40, 60, 80, and 100% semispan stations, respectively. Therefore, the total number of design variables was 10. The acceptable range of these design variables is described in Table 2.

2. Objective and Constraints for the Optimization

The definition of the objective and that of the constraints were the same as that of the preceding optimization of section airfoil shape. The objective was to minimize C_{DP}, which was computed by the Euler code at a cruising Mach number of 0.98. The constraint that C_L kept constant (0.26) was realized by adjusting the angle of attack. Another constraint, namely, that the wing volume of the designed airplane should be greater than that of NEXST-1, was also set.

B. Results and Discussion

For the optimization, GA was used. The population size at each generation was set to be 20, the probability of mutation was 0.1, and all initial individuals were randomly generated. The computation was done until the 30th generation, so that about 600 flow simulations of different shaped airplanes were required. The unstructured mesh generation and the aerodynamic evaluation of one individual demanded about two hours for the computation using NEC SX-7.

The evolutional process of the planform shape is shown in Fig. 12. The airplane shape evolved from the left (beginning stage) to the right (matured stage). At first, the geometries of the beginning stage were almost randomly one and strange on the whole. Then the sweep angle gradually increased with the evolutionary computation, and finally the geometries of the matured stage converged on an almost conventional SST configuration. The aerodynamic performance of NEXST-1 and that of the obtained optimal design are compared in Table 3. Keeping the wing volume and C_L constant, 17 counts of reduction of C_{DP} were achieved. The performance of the optimal design is compared with that of NEXST-1 in the following section.

1. Comparison About the Geometry

The planform shape of the final optimal design is shown in Fig. 13 with that of NEXST-1. A 13% increase of the aspect ratio (AR) and the modification of the wing planform shape from double delta to as like delta wing were observed. Moreover, it was confirmed that the twist angle distribution was almost same as that of NEXST-1.

Table 3 Comparison of the aerodynamic performance of planform shape optimization

Design	Wing volume	AR	Evaluation	AoA, deg	C_L	C_{DP}	$L/D_{inviscid}$
NEXST-1	1.000	2.20	Euler	3.48	0.26	0.01855	14.02
Planform optimal	1.047	2.48 +13%	Euler	3.29	0.26	0.01689 −17 counts	15.40 +9.8%

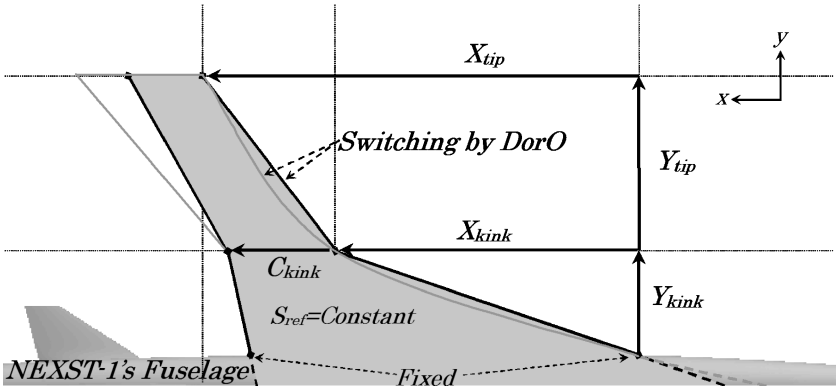

Fig. 11 Design variables definition for planform shape optimization.

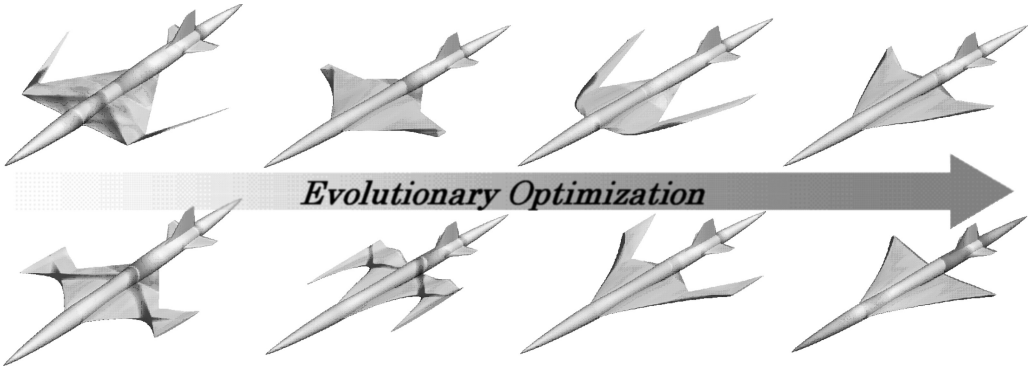

Fig. 12 Evolutional process of the planform shape.

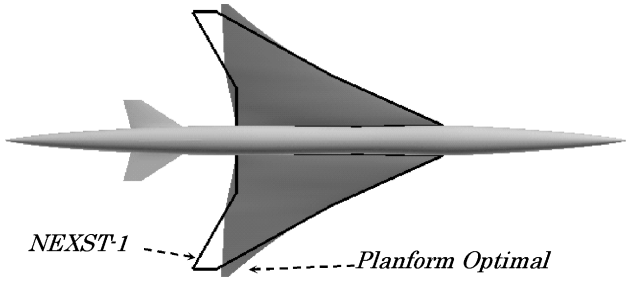

Fig. 13 Geometry of the planform optimal design.

The section area distribution normal to the freestream flow direction of the obtained optimal design is shown in Fig. 14. It was confirmed that the distribution varied more rapidly at the trailing-edge position (x/length ~ 0.63) by the modification of the geometry from the double-delta wing to the delta wing. So it was considered that this result showed the tradeoff relation between the smoothness of the area distribution (wave drag reduction) and the increase of the aspect ratio (induced drag reduction).

2. Comparison About the Aerodynamics

The lift and pressure drag force distributions in the spanwise direction are shown in Fig. 15. The spanwise lift distribution was modified so as to be more elliptical than that of NEXST-1. The spanwise pressure drag force was reduced almost constantly at all span stations.

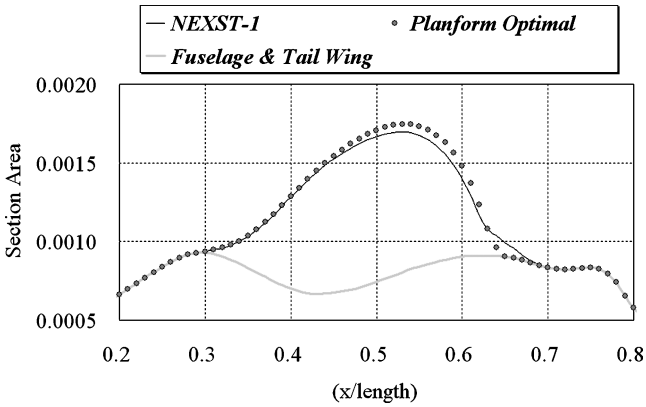

Fig. 14 Area rule investigation for the planform shape optimization.

Comparison of Cp distribution at the 40% semispan station and the visualization of the shock location with the entropy production are shown in Figs. 16 and 17, respectively. The same manner of shock visualization of the NEXST-1 model is included in Fig. 6. The shock location was considered to be almost the same as that of NEXST-1, and the shock strength was also almost the same as that of NEXST-1.

The formula of the classical induced drag prediction based on the lifting-line theory is given as follows:

$$C_{D\_Induced} = C_L^2 \big/ (\pi \cdot AR \cdot e) \tag{2}$$

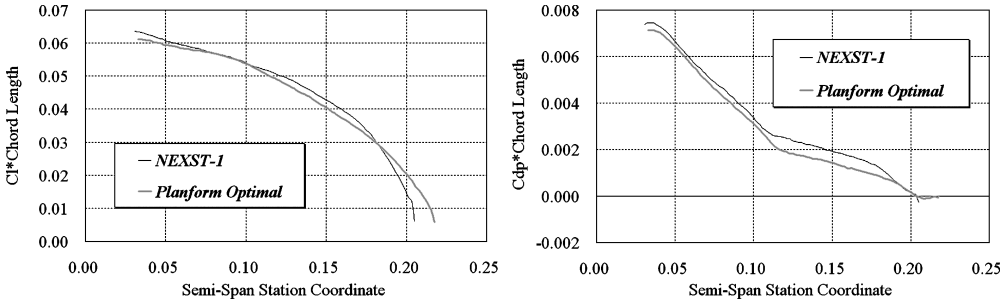

Fig. 15 Lift and pressure drag distributions of planform optimal design in the spanwise direction.

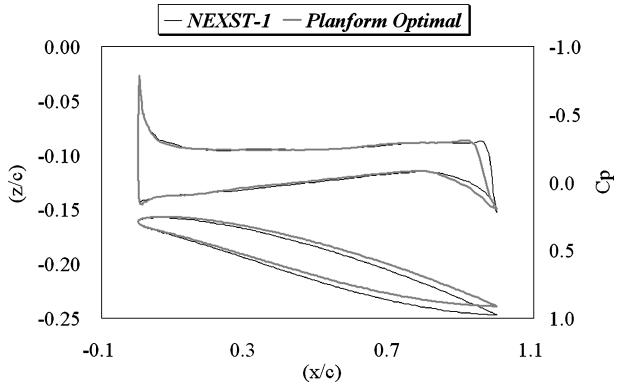

Fig. 16 *Cp* distribution of planform optimal design at 40% semispan.

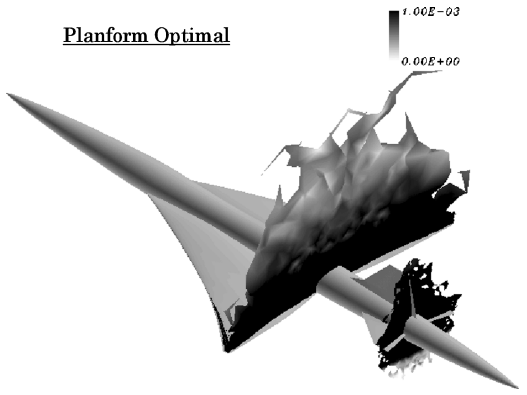

Fig. 17 Shock and entropy visualization.

The induced drag reduction caused by the increase of the aspect ratio was estimated to be about 14 counts by the lifting-line theory (e was assumed to be 0.8). This drag reduction level almost agreed with that achieved by the present planform shape optimization. Therefore, it was concluded that the induced drag was mainly reduced in the present optimization while the wave drag was kept almost constant.

V. Validation Study and Further Investigation

Comparison of C_{DP}-Mach curves of NEXST-1 and the two optimal designs obtained in this research at $C_L = 0.26$ is presented in Fig. 18. The drag minimum region, which appeared in the near-sonic regime, is called drag bucket. From the figure, good off-design performance of the two optimal designs was confirmed. In the whole range of the transonic and the near-sonic regimes, improvement in the aerodynamic performance was achieved. The optimized performance achieved in the planform shape optimization was inferior to that achieved in the section airfoil shape optimization. The reason why excellent improvement was not achieved by the planform shape optimization was thought to be the result of the strong constraints such as the S_{ref}, wing volume, and t/c constant as well as the fixed wing-root length.

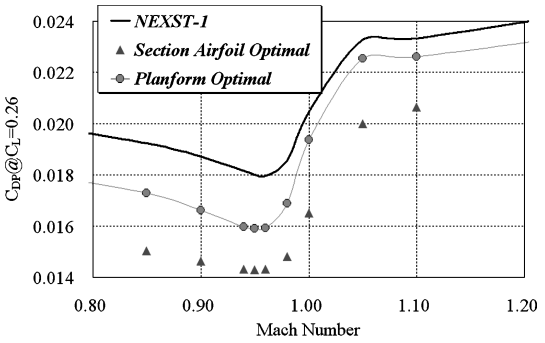

Fig. 18 Drag bucket at $C_L = 0.26$.

Moreover, the mesh dependency effect and the viscous flow effect (i.e., NS computation) were also analyzed. Results of these analyses also supported the validity of the present optimizations on the whole. The Euler computational result using a fine unstructured mesh (about 2.5 millions nodes) and the NS computational result of the section airfoil shape optimization are included in Table 1. The same level reduction of C_{DP} as that of the original Euler computation was confirmed in both cases.

VI. Conclusions

In this paper, two aerodynamic shape optimizations of a near-sonic airplane were conducted using a genetic algorithm with an unstructured mesh flow simulation method. One was section airfoil shape optimization, and the other was planform shape optimization. For both optimizations, the NEXST-1 supersonic transport model was used as the baseline model. To enhance the efficiency and the robustness of the optimization, the mesh-movement method and the automatic unstructured mesh-regeneration system were applied in the optimizations.

By the section airfoil shape optimization, significant C_{DP} reduction was achieved. It was confirmed that the wave drag was greatly reduced in this optimization. Wing surface geometry causing isentropic compression at the upstream region of shock wave was an important factor for C_{DP} reduction in the near-sonic regime. Moreover, the optimized position of the pressure recovery associated with the crest position on the outboard wing upper surface realized thrust pressure force in the optimal design. In short, the washout of the main wing around the tip caused thrust force.

Another C_{DP} reduction was achieved by the planform shape optimization. In this optimization, the induced drag was largely reduced while the wave drag was kept almost constant. The optimal planform shape almost converged on a delta wing one for an increase of the aspect ratio and for maintenance of the sweep angle.

In the present study, the important factors for reduction of the drag force of a near-sonic airplane were separated. To reduce the induced drag component of the total drag, the planform should be modified. On the other hand, to reduce the wave drag component, the shape of the section airfoil should be optimized. Therefore, with the full shape optimization, including the wing section, planform, and fuselage design, it will be feasible to realize an efficient near-sonic airplane whose lift-to-drag ratio is similar to that of conventional transonic transport.

References

[1]Sakata, K., "Supersonic Experimental Airplane (NEXST) for Next Generation SST Technology," AIAA Paper 2002-0527, Jan. 2002.

[2]Matsushima, K., Iwamiya, T., and Ishikawa, H., "Supersonic Inverse Design of Wings for the Full Configuration of Japanese SST," *Proceedings of the 22nd ICAS Congress*, International Council of the Aeronautical Sciences, 2000, pp. 213.1–213.8.

[3]Matsushima, K., Iwamiya, T., and Nakahashi, K., "Wing Design for Supersonic Transports Using Integral Equation Method," *Engineering Analysis with Boundary Elements*, Vol. 28, No. 3, 2004, pp. 247–255.

[4]Becker, V. J., "The High Speed Frontier," NASA SP-445, 1980, pp. 36–59, 84–117.

[5]Haines, B., "The Aerodynamic Design of the Wing–Fuselage for a Near-Sonic Transport," AIAA Paper 2002-0517, Jan. 2002.

[6]"Boeing Fights to Revive Sonic Interest," *Flight International*, Vol. 162, No. 4850, 2002, p. 6.

[7]Matsushima, K., Yamazaki, W., and Nakahashi, K., "Transonic Design of SST—To Employ Japanese SST as a Candidate for Near Sonic Transport," *Fluid Mechanics and Application*, Vol. 73, Kluwer Academic, 2003, pp. 317–324.

[8]Takenaka, K., Yamamoto, K., and Takaki, R., "CFD Validation Study of NEXST-1 Near Mach 1," *Proceedings of the 24th ICAS Congress*, International Council of the Aeronautical Sciences, 2004, pp. 361.1–361.8.

[9]Fonseca, C. M., and Fleming, P. J., "Genetic Algorithms for Multiobjective Optimization: Formulation, Discussion and Generalization," *Proceedings of the 5th ICGA*, 1993, pp. 416–423.

[10]Obayashi, S., and Guruswamy, G. P., "Convergence Acceleration of a Navier–Stokes Solver for Efficient Static Aeroelastic Computations," *AIAA Journal*, Vol. 33, No. 6, 1995, pp. 1134–1141.

[11]Venkatakrishnan, V., "On the Accuracy of Limiters and Convergence to Steady State Solutions," AIAA Paper 93-0880, Jan. 1993.

[12]Sharov, D., and Nakahashi, K., "Reordering of Hybrid Unstructured Grids for Lower–Upper Symmetric Gauss–Seidel Computations," *AIAA Journal*, Vol. 36, No. 3, 1998, pp. 484–486.

[13]Ito, Y., and Nakahashi, K., "Surface Triangulation for Polygonal Models Based on CAD Data," *International Journal for Numerical Methods in Fluids*, Vol. 39, No. 1, 2002, pp. 75–96.

[14]Sharov, D., and Nakahashi, K., "Hybrid Prismatic/Tetrahedral Grid Generation for Viscous Flow Applications," *AIAA Journal*, Vol. 36, No. 2, 1998, pp. 157–162.

[15]Ito, Y., and Nakahashi, K., "Improvements in the Reliability and Quality of Unstructured Hybrid Mesh Generation," *International Journal for Numerical Methods in Fluids*, Vol. 45, No. 1, 2004, pp. 79–108.

[16]Goldberg, U. C., "Toward a Pointwise Turbulence Model for Wall-Bounded and Free Shear Flows," *Journal of Fluids Engineering*, Vol. 116, No. 1, 1994, pp. 72–76.

[17]Murayama, M., Nakahashi, K., and Matsushima, K., "Unstructured Dynamic Mesh for Large Movement and Deformation," AIAA Paper 2002-0122, Jan. 2002.

[18]Paparone, L., and Tognaccini, R., "Computational Fluid Dynamics-Based Drag Prediction and Decomposition," *AIAA Journal*, Vol. 41, No. 9, 2003, pp. 1647–1657.

R. So
Associate Editor